To refer to or to cite this work, please use the citation to the published version:
Missinne, Jeroen, et al. "Compact packaged silicon photonic Bragg grating sensor based on a ball lens interface." Optics & Laser Technology 157 (2023): 108768. https://doi.org/10.1016/j.optlastec.2022.108768

Highlights

Compact packaged silicon photonic Bragg grating sensor based on a ball lens interface

Jeroen Missinne, Viktor Geudens, Steven Van Put, Giannis Poulopoulos, Michal Szaj, Charalampos Zervos, Hercules Avramopoulos, Geert Van Steenberge

- Low-loss ball lens interface for fiber-to-grating coupling from the back side
- Precision fused silica ball lens holder realized using laser direct-write technology
- Phase-shifted Bragg grating sensors read out efficiently in reflection with ball lens
- Compact packaged silicon photonic Bragg grating temperature sensor demonstrated
- The temperature sensitivity in the tested range was 73 pm/°C.

Compact packaged silicon photonic Bragg grating sensor based on a ball lens interface

Jeroen Missinne[a,*], Viktor Geudens[a], Steven Van Put[a], Giannis Poulopoulos[b], Michal Szaj[c], Charalampos Zervos[b], Hercules Avramopoulos[b], Geert Van Steenberge[a]

[a] *Center for Microsystem Technology (CMST), Ghent University and imec, Technologiepark 126, Zwijnaarde, 9052, Belgium*
[b] *Photonics Communications Research Laboratory,National Technical University of Athens, 9 Iroon Polytechniou Street, Zografou Athens, 15773, Greece*
[c] *Argotech a.s., Náchodská 529, Trutnov, CZ-541 01, Czech Republic*

Abstract

We demonstrate a ball-lens based optical interface for coupling between a single mode fiber and a silicon grating coupler from the back side of a photonic integrated circuit (PIC). This allows compact packaging solutions and keeps the PIC top side accessible, e.g. for interacting with the environment in case of sensing applications. Different configurations employing 300 μm diameter ball lenses made of both LASF-35 glass and sapphire were investigated. Without any modifications to the grating coupler, the peak coupling efficiency (for TE polarization and operating wavelength around 1550 nm) was experimentally found to be only between 1.4 dB and 2.2 dB lower when interfacing with a ball lens from the back side compared to coupling from the top side using a cleaved fiber. Furthermore, no noticeable change in the bandwidth was found. The potential of the ball lens interface was proven by realizing a compact (diameter less than 1.5 mm) optical temperature sensor probe based on a phased shifted silicon photonic Bragg grating structure on a PIC. The probe consisted of a single mode fiber which was terminated with a 1.25 mm ceramic ferrule onto which a ball lens holder and a PIC was glued. The holder was realized in fused silica glass with a femtosecond laser direct-write technology and served to accurately position the ball lens with respect to the fiber and PIC. The assembly allowed to cleanly read out the Bragg grating spectrum in reflection, using a single fiber interface and was compatible with commercial interrogator systems. A Bragg wavelength shift of 73 pm/°C was found in a tested temperature range between 15°C and 60°C.

Keywords:
ball lens, Bragg grating sensor, coupling, femtosecond laser, optical interface, packaging, photonic integrated circuit, sensor probe, silicon photonics

1. Introduction

Silicon photonics is rapidly gaining interest, not only for datacom and telecommunication applications [1, 2], but also for sensing [3, 4, 5, 6, 7]. One of the clear advantages of this technology is that optical circuits can densely be integrated on such a Photonic Integrated Circuit (PIC). However, since PICs typically rely on sub-micrometer-sized waveguides, the packaging process (e.g. attaching fibers or light sources and detectors) is not only challenging, but also one of the most costly processes required to realize a photonic product. A common practice in packaging is to precisely align and glue a fiber (array) on the PIC top surface as a way to interface upwards emitting grating couplers [8]. In case edge couplers are implemented, the fiber array can be mounted at the chip edge thereby keeping the PIC surface accessible [9]. As an alternative to direct fiber attachment, intermediate micro-optical components have been used, e.g. microlens arrays mounted on top of the grating couplers as an interface between the fiber and PIC [10], micro-optical benches employing 2 ball lenses for hybrid integration of a laser onto a PIC [11], or in situ printed free-form coupling elements [12]. The disadvantage of the above-mentioned approaches in which the PIC is interfaced from the top side is that part of the surface is blocked, which especially for sensing applications may be an issue since it hinders the interaction between sensor structures on the PIC and the environment. The opportunity of using intermediate micro-optics is that the working distance can be increased, so that grating couplers on the PIC can be interfaced through the substrate from the back side, thereby keeping the top surface free for sensing. We have previously reported on a technique to interface a PIC with a single mode fiber from the back side using integrated microlenses [13, 14]. This approach is particularly advantageous when interfacing an array of grating couplers but requires lithographic definition and etching of microlenses on the back side of the PIC which is a significant post-processing effort that can most reliably be performed at wafer-level. An alternative solution for back side coupling which does not require post-processing (apart from a back side polishing step and the application of an anti-reflection coating) is using a ball lens [15]. Although a typical ball lens has a larger size (300 μm in the current paper) than a microlens and may therefore be less ideal for interfacing densely spaced grating coupler arrays, the approach is a low-complexity solution in case of single grating coupler interfacing. Furthermore, since this approach does not require lithographic post-processing, it could be a potentially very interesting solution for small-volume production or for prototyp-

*Jeroen.Missinne@UGent.be

ing using multi-project wafer PICs, which are received as small, diced pieces rather than in full wafers. Compared to previous work [15], we report on a ball lens solution for back side coupling to a PIC in which the single mode fiber can be mounted perpendicularly to the surface which allows a low-complexity and compact packaging solution. Additionally, we perform a detailed study of the coupling performance and compare 2 ball lens configurations and ball lens materials. We also demonstrate the concept by realizing a packaged silicon photonics sensor probe. As sensing element, a PIC with a Bragg grating is chosen since it is a proven sensor concept and this structure can be read out in reflection, thereby requiring only a single grating coupler. Bragg grating sensor elements in optical fibers [16] are widely commercially available and are commonly used for reliable strain and temperature sensing. Alternatively, Bragg gratings implemented in a silicon waveguide on a PIC have been reported for biochemical sensing [17, 18, 19] and temperature sensing [20]. The advantage of PIC-based over fiber-based Bragg grating sensors is that they can be much shorter and can achieve higher sensitivity, e.g. for temperature [20]. Furthermore, because of the wafer-scale fabrication process, PICs can potentially be produced at very low cost and owing to advanced patterning capabilities and the availability of a whole range of sensor materials, there is a large parameter space for optimizing the sensor towards a specific application. On the other hand, PIC-based Bragg grating sensors typically have a wider spectral bandwidth, which limits the accuracy in determining the Bragg wavelength. Furthermore, PIC-based Bragg grating sensors require a fiber connection, which makes their packaging and interconnection more complex. Herein, we implement the back side ball lens coupling approach for reading out Bragg grating sensor signals and we demonstrate a very compact eventual sensor probe with a diameter less than 1.5 mm. Furthermore, this type of optical sensor is plug-in compatible with commercially available interrogators currently used for reading out fiber Bragg grating sensors. As an example, a Bragg-grating based temperature sensor probe is realized, but the concept can be extended to other types of sensors e.g. measuring refractive index

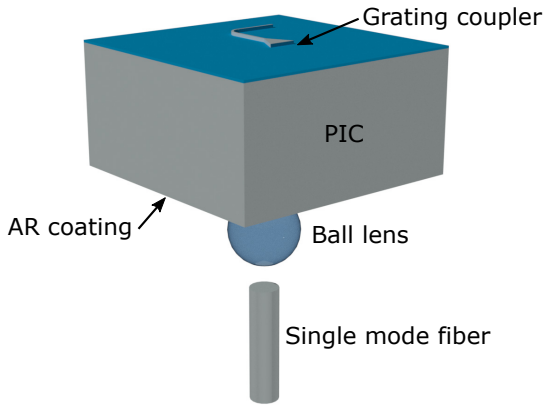

Figure 1: Schematic illustration of the ball lens coupling concept which allows interfacing a grating coupler from the back side of the PIC. The ball lens holder is not shown on this sketch for clarity. The PIC used for the demonstrator measures 1 mm x 1 mm x 0.73 mm while the ball lens measures 300 µm in diameter.

2. Design and Methods

2.1. Overall concept

The overall concept of the optical interface is to use a ball lens to focus the diverging beam emitted by the fiber onto the grating coupler. This allows efficiently bridging the distance between the fiber and grating coupler and thus allows interfacing the PIC from the back side, as schematically illustrated in Figure 1. By laterally shifting the ball lens with respect to the central axis of the fiber, the beam will deflect and be incident on the grating coupler at the desired angle while the fiber itself remains perpendicular to the PIC surface thereby facilitating the packaging process.

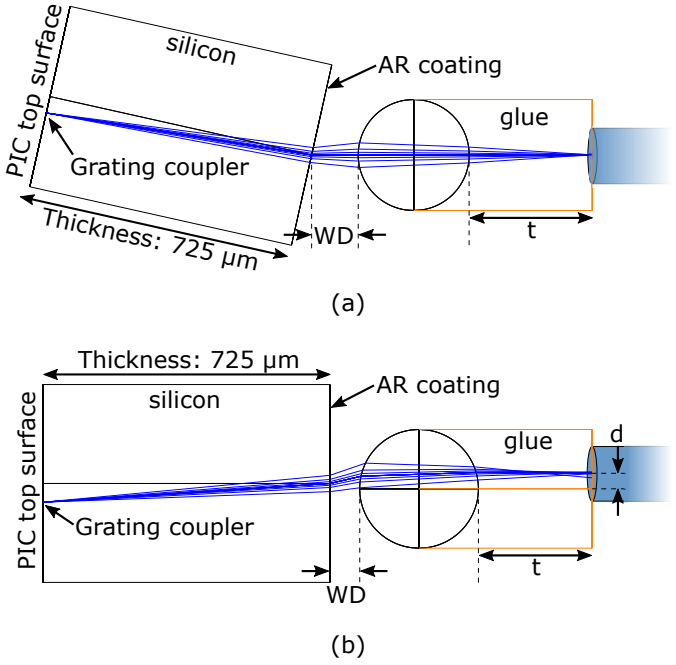

Figure 2: Cross-sectional view on the coupling configuration showing a schematic illustration of the ball lens designs as optimized in Zemax OpticStudio: (a) in-line configuration and (b) shifted ball lens configuration. The diameter of the ball lens was 300 µm, the refractive index of the glue was 1.54 (at λ = 1550 nm) and the design parameters are tabulated in Table 1 for both sapphire and LASF-35 lenses

2.2. Design of the sensor optical interface

The ball lens optical interface design is based on a lens system in which the light focused by the ball lens forms a spot on the grating coupler having the same mode field diameter (MFD) as emitted by the fiber, assuming the grating coupler is optimized for such MFD.

Since a single ball lens is used, the design is rather straightforward and consists of placing the ball lens at the correct position with respect to the fiber facet and grating coupler. Here, a standard 300 µm diameter ball lens was chosen to achieve a compact package. Even smaller ball lenses are less common and therefore difficult to obtain. In this paper, two different types of ball lens materials are explored, i.e. sapphire and LASF-35 glass (obtained from Sandoz, Switzerland). For

Table 1: Design parameters of the ball lens configurations as defined in Figure 2

	Sapphire ball lens		LASF-35 ball lens	
	in-line	shifted	in-line	shifted
Glue thickness (t) [μm]	333	287	226	198
Working distance (WD) [μm]	123	75	22	5
Lateral lens displacement (d) [μm]	0	40	0	32.5
AR coating	no	no	yes	yes
Simulated coupling efficiency [dB]	-0.54	-1.14	-0.29	-0.35

initial experimental validation of the concept, commonly available 300 μm sapphire ball lenses were used. However, sapphire is birefringent, which makes it a less ideal material choice in combination with polarization selective grating couplers on the PIC. Therefore, also ball lens interfaces with the LASF-35 high refractive index glass (n = 1.975 at λ = 1529.6 nm) were implemented. The sapphire ball lenses used in this work were uncoated, while the LASF-35 ball lenses had an anti-reflection coating against air.

Zemax OpticStudio was used to optimize the design parameters at a design wavelength of 1550 nm. Cross-sections of the 2 coupling configurations that were investigated are shown in Figure 2: (a) a ball lens in-line, or centered on the axis of the optical fiber and (b) a ball lens laterally shifted with respect to the fiber. In the in-line configuration, the 10.4 μm spot emitted by the single mode fiber is replicated at a certain position in front of the lens. This allows bridging the 725 μm PIC substrate thickness, however, the fiber with ball lens should be tilted with respect to the PIC surface to obey the required grating coupler angle, thereby complicating the packaging process. In the shifted-lens configuration, the ball lens is laterally displaced from the fiber axis, thereby additionally deflecting the beam at the required angle. This allows attaching the fiber-ball-lens assembly perpendicularly to the PIC surface. A ray-based model is shown in Figure 2 for illustrative purpose, however, the optimization itself was performed using the "Physical Optics Propagation" module based on Gaussian beam propagation. Here, the design was optimized to operate around 1550 nm wavelength and for a grating coupling angle of 12.5°, but can easily be modified to operate at slightly different conditions. Although grating couplers operating at the default 10° coupling angle were targeted, we measured that the fabricated grating coupler spectra were not centered near 1555 nm (as desired) at this coupling angle, but rather around longer wavelengths due to PIC fabrication inaccuracies. Therefore, a larger coupling angle was used throughout the paper to compensate for this, resulting in a grating coupler spectrum around 1555 nm as targeted. Because of the limited amount of design parameters, the optimization was performed using a manual iterative process. The design parameters after optimization are summarized in Table 1 for configurations (a) and (b) and for both types of ball lenses investigated. Taking into account the future packaging process, the design assumes a glue (with refractive index 1.54 at λ = 1550 nm) between the fiber end face and ball lens, and air between the ball lens and PIC back side. The simulated coupling efficiencies, listed in Table 1, are obtained by calculating the overlap integral (using OpticStudio) between the propagated beam and an ideal Gaussian mode profile, and therefore only takes into account the lens system, not the efficiency of the specific grating coupler used. It can be seen that the coupling efficiencies for the shifted configurations are lower, which is due to increased impact of spherical aberration for this off-axis behavior causing a phase mismatch and a non-Gaussian intensity profile. Likewise, aberrations are higher for the sapphire compared to the LASF-35 ball lens system.

2.3. Coupling performance of the ball lens interface

To assess the coupling performance towards a grating coupler on a PIC, test structures were used consisting of short sections (0.5 mm) of straight 450 nm wide, 220 nm thick Si strip waveguides having a TE grating coupler (nominal design: 625 nm pitch, 50% duty cycle, 70 nm etch depth) on each side, fabricated in the imec Passives+ technology (ISIPP50G) using the multi-project wafer (MPW) service. The Si waveguides and grating couplers were fully covered with oxide over-cladding. The waveguide section also included a Bragg grating sensor, as discussed below. A 12.5° coupling angle was used for all measurements discussed in this publication (unless otherwise mentioned), as already explained above. To allow interfacing, the otherwise rough PIC back side was polished and a single layer anti-reflection coating (silicon nitride, thickness 200 nm) was deposited to improve coupling efficiency by 1.5 dB, as previously experimentally verified (at 1310 nm wavelength) [21].

As a reference, the total insertion loss between input fiber, over waveguide, to output fiber (both fibers interfacing the PIC from the top side) was recorded. For obtaining ball lens coupling efficiencies, the bare fiber at the input grating coupler was replaced by a ball lens interface, aligned below the grating coupler at the back side of the PIC. The ball lens interfaces employed for this experiment were realized by aligning and gluing sapphire and LASF-35 ball lenses directly above a single mode fiber mounted in a ferrule according to the in-line and shifted design configuration (cfr. Figure 2 and Table 1). The input reference fiber or fiber with glued ball lens was connected, over a 3-paddle polarization controller, to a superluminescent diode (SLED) with a 65 nm 3 dB bandwidth centered around 1550 nm (Exalos EXS1510-1110) and the receiving fiber was connected to an optical spectrum analyser (OSA, Agilent 86142B). Several ball lens configurations were compared, i.e. the in-line configuration (sapphire ball lens) and the shifted configuration (sapphire and LASF-35).

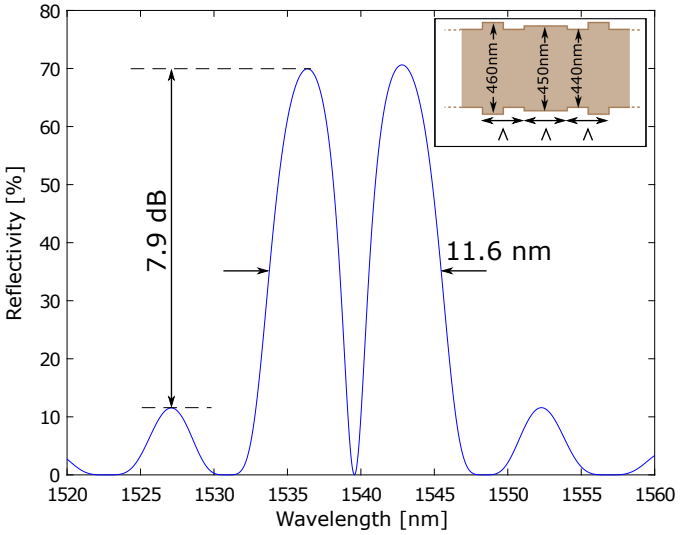

Figure 3: Simulated reflection spectrum of the phase shifted Bragg grating sensors (pitch Λ = 326 nm). The inset illustrates the layout (top view) of the designed component at the phase shifting region in the center. The widths of the different sections are indicated while the thickness is constant (220 nm).

2.4. Bragg grating sensor design

For demonstration purpose, Bragg gratings were selected as precise sensor elements, because they can be read out in reflection, which requires only 1 optical fiber and therefore allows realizing a very compact packaged sensor probe. In addition, Bragg grating sensors can be multiplexed in the spectral domain, meaning that multiple sensors can be read out using the same fiber. A Bragg grating shows a peak in the reflection spectrum which is centered around the Bragg wavelength λ_B, defined as $\lambda_B = 2\Lambda n_{eff}$, with Λ being the grating pitch and n_{eff} the effective refractive index in the grating section [16]. Bragg gratings were realized by implementing side wall corrugations to the silicon waveguides. Because of the large coupling coefficient of such gratings, their bandwidth is relatively wide. However, narrow bandwidths are preferred to allow accurate peak tracking in the spectral domain. Therefore, a phase-shifted Bragg grating was designed, i.e. a Bragg grating in which a π-phase shift is introduced between 2 identical Bragg grating sections. The reflection spectrum of such a component theoretically shows a narrow Lorentzian-shaped dip (with a much smaller bandwidth), in the center of the grating reflection spectrum. The Bragg grating design was optimized based on propagation simulations employing the EigenMode Expansion (EME) module of Mode Solutions (Ansys Lumerical), obtaining the reflection spectra of these components varying several design parameters (pitch Λ, corrugation width, number of periods). The designed component is composed of an intermediate region with two Bragg gratings on each side. This intermediate region acts as a defect between the two Bragg gratings and has a length equal to the grating pitch and nominal width of 450 nm (i.e. the waveguide width), forming a Fabry-Perot cavity with mirrors formed by the gratings on each side. This π-phase shift results in a resonance dip within the passband of the reflection spectrum. After optimization, the Bragg grating design parameters were fixed, i.e. a sidewall corrugation width of 20 nm on a nominal waveguide width of 450 nm, and a length of 200 periods. More details on the sensor design can be found in [22]. The sidewall corrugated sections were found to support a fundamental TE polarisation mode with effective refractive index values of 2.3271 and 2.3699, for waveguide section widths of 440 nm and 460 nm, respectively. The simulated reflection spectrum for the design with grating pitch 326 nm is shown in Figure 3, together with a schematic representation of the component layout. The difference between peak grating reflectivity and the reflectivity of the first side lobe was calculated to be 7.9 dB. The envelope 3-dB bandwidth (ignoring resonance dip) was calculated to be 11.6 nm. Since the Bragg wavelength λ_B is very sensitive to changes in n_{eff}, which in turn is very sensitive to changes in the refractive index and thickness of the silicon waveguide, sensors with grating pitches 324 nm and 328 nm were also implemented, to ensure having test structures in the suitable spectral range. Those variations yield nearly identical reflection spectra, but 5.2 nm blue-shifted or red-shifted in Bragg wavelength respectively. The simulated shift in Bragg wavelength as a function of temperature was previously reported to be 70 pm/° C [22] for the adopted technology.

After receiving the fabricated PIC according to the design, the Bragg grating reflection spectra were experimentally recorded by interfacing a single grating coupler on the test structures in reflection with a ball lens from the PIC back side. Therefore, a polarization independent circulator (Thorlabs 6015-3-APC) was added to the setup. The SLED with polarization controller was connected to port 1, the ball lens interface to port 2, and the optical spectrum analyser to port 3 of the circulator. As a comparison, reflection spectra were also recorded from the top side using a bare fiber instead of the ball lens. In that case, an index matching liquid (Cargille liquid with a refractive index 1.45 at λ = 1550 nm and T = 25°C) was dispensed between the cleaved fiber tip and the top side of the PIC to avoid parasitic reflections at the two silica-air interfaces and in that case the applied coupling angle was reduced to 12.5°/1.45 = 8.6°. The circulator insertion loss was taken into account in the calculation of the reflectivity spectra.

2.5. Realization of a precision ball lens holder

After the validation experiments, a robust optical interface was realized which involved fabricating a suitable holder in which a commercial ball lens can be mounted and precisely aligned with respect to both the interfacing fiber and the PIC. Here, we propose a conically-shaped cavity as ball lens holder, drastically improving the ball lens positioning accuracy compared to a laser-ablated through-via realized in previous work [15]. By controlling the slope and dimensions of the conical cavity, the ball lens can be positioned at the desired x, y and z coordinates as dictated by the design.

For fabricating this 3D holder with micrometer resolution, the FLICE (Femtosecond-Laser Irradiation followed by Chemical Etching) technology was adopted. This technology relies on irradiating fused silica glass with a tightly focused fs-laser spot which is scanned in the bulk of the glass according to a

3D CAD drawing. As a result, the etch rate (in KOH etchant) of the irradiated zones increases drastically compared to the non-exposed glass. This is an established technique which has previously been applied e.g. for the fabrication of optofluidics [23], optical switches [24], V-grooves for fiber alignment [25], and optical resonators [26]. For the current work, the FLICE technology was further optimized specifically for achieving a conical holder with a 45° slope angle. By optimizing the position of the cone in the depth (z-direction), the desired distance between the ball lens and fiber was achieved. Note that below the conical holder, in the area between the ball lens and optical fiber, a cylindrical cavity (diameter approximately 150 μm) was implemented which will be filled with a glue according to the design. This ensures a single and uniform interface between the fiber end face and ball lens.

A commercial ytterbium-doped fiber laser having a pulse length <400 fs (Satsuma, Amplitude Systèmes) was used to realize the holder. The lasing wavelength of 1030 nm was frequency doubled to 515 nm using a second harmonic generation module (Satsuma, Amplitude Systèmes) and the polarization was converted to circular polarization by inserting a quarter waveplate in the beam path. The pulse repetition rate was set to 500 kHz and the circularly polarized beam was focused into a high purity, nominally 500 μm thick fused silica substrate (supplier: Siegert Wafer) using a 0.55 NA aspheric lens (Newport 5722-A-H). The glass substrate was placed on a motorized XY stage allowing transverse writing while the aspheric lens was mounted on a vertical translation stage to control focusing depth.

The cone was realized by writing a series of concentric circles with increasing diameter from bottom to top. At each z-position, 3 concentric circles were written (translation speed: 1 mm/s, pulse energy 200 nJ) with a lateral line-to-line pitch of 2 μm. Then, the aspheric lens was moved 2 μm up and similarly, each time 3 concentric circles (with increased diameter) were written. The procedure was repeated until the top surface of the glass was reached and the diameters of the circles at the different z-positions were defined so that the desired 45° slope angle was obtained. The cylindrical cavity at the bottom, was defined by moving the laser spot in a spiraling path from bottom to top (spiral diameter 150 μm, in-plane writing speed 1 mm/s, vertical translation speed: 0.002 mm/s).

After laser exposure, the glass was submerged in a 30 % KOH solution heated at 85°C and continuously mixed with a magnetic stirrer. The total etching time was 8 h. For inspection of the realized structures after etching, cross-sections were made using a wafer dicer equipped with a diamond coated blade and inspected using a microscope.

2.6. Proof-of-concept sensor demonstration

After optimizing the holder fabrication process, functional sensor assemblies were produced to prove the concept of the ball lens optical interface to obtain very compact (diameter <1.5 mm) PIC-based optical temperature sensor probes. The demonstrator was realized employing a 300 μm sapphire ball lens and to facilitate packaging, holders were fabricated according to the laterally shifted design. After holder fabrication, first, the ball lenses were fixed in the holders using a UV-curable epoxy. Then, the holders were diced to the required dimensions (970 μm x 970 μm). For this design, an additional spacer was required to ensure a proper working distance between ball lens and PIC after assembly. Therefore, a circular opening was realized (using the FLICE technique) in a 130 μm thick fused silica glass slide, which was glued on the holder to act as spacer. Subsequently, the holder assembly was precisely aligned above and glued to a single mode fiber (SMF-28 housed in a 1.25 mm diameter ceramic ferrule) at the lateral coordinates dictated by the design. Finally, the PIC (size: 970 μm x 970 μm, 725 μm thickness) was aligned above the fiber+holder assembly using a precision gripper mounted on a translation stage. The initial alignment was performed based on the component outlines, and final alignment was achieved by actively monitoring the reflected sensor signal using the same circulator-based setup as described above. Once aligned, small drops of epoxy were applied at the holder-PIC interface from the sides, and cured using UV light. Note that for the proof-of-concept demonstration, a different PIC with a different phase shifted Bragg grating sensor (i.e. with a 324 nm pitch) was used than the one for the above-mentioned experiments.

The sensor functionality and sensitivity was tested by subjecting it to temperatures between 15°C and 60°C in steps of 5°C using a climate chamber (Vötsch VTS 7040-15). To this end, the complete assembled sensor was placed in the center of the chamber. The optical fiber was led out of the chamber through a dedicated opening, and connected to an FBG-scan 608 Bragg grating interrogator located outside the testing chamber. As a reference, a type K thermocouple sensor was placed in the chamber next to the sensor under test and it was read out using a Pico USB TC-08 controller (also located outside the chamber). Each time the temperate was stabilized, the thermocouple was read out and 5 identical Bragg grating spectra were obtained from the interrogator. For each individual recording, the dip in the spectrum was fitted to a Lorentzian function from which the Bragg wavelength was obtained as the wavelength at minimum intensity. For each temperature, the Bragg wavelength averaged over 5 fitted spectra was plotted as a function of recorded thermocouple values.

3. Results and discussion

3.1. Evaluation of the ball lens coupling efficiency

Figure 4 plots the fiber-to-fiber coupling efficiencies of the reference configuration (black curve) together with 3 configurations in which one of the fibers was replaced by a ball lens interface coupling to the grating from the back side. Note that the typical phase shifted Bragg grating sensor signature is visible in the transmission spectra around 1536 nm wavelength. If the propagation loss in the 0.5 mm long waveguide section is neglected, a -5 dB peak coupling efficiency per grating coupler was obtained for top side coupling with bare fibers (reference). Although this is slightly lower than specified for this type of grating coupler (i.e. -4.3 dB), this value will only be used as a reference to evaluate ball lens interface performance in the current paper.

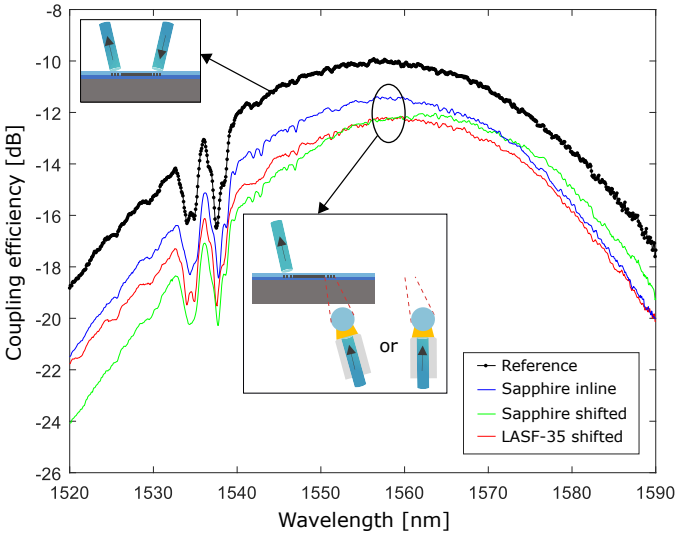

Figure 4: Fiber-to-fiber coupling efficiency spectra for the reference configuration (both TE grating couplers interfaced from the top side using cleaved fibers) and 3 different ball lens configurations (1 grating coupler interfaced with a ball lens from the back side). The environmental temperature was kept fixed at 22°C and coupling angle was set to 12.5° for all configurations.

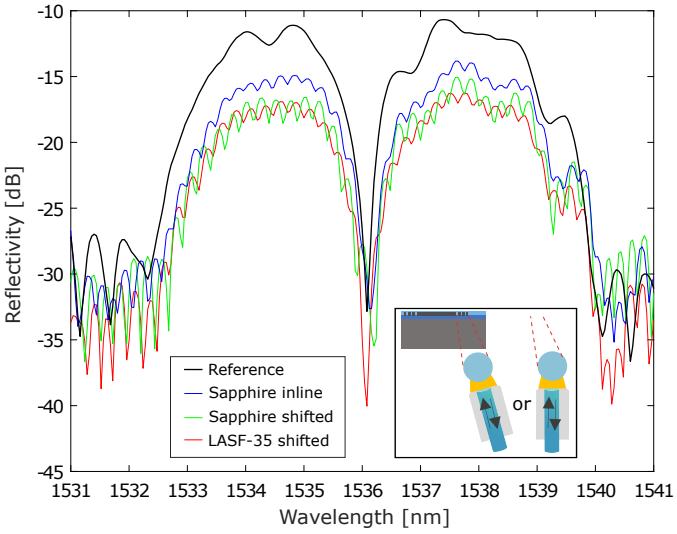

Figure 5: Reflection spectra of the 326 nm pitch phase shifted Bragg grating temperature sensor recorded at 22°C using 3 different ball lens interfaces from the back side (coupling angle 15°) and using a bare fiber with index matching liquid from the top side (reference, coupling angle 10.3°).

When the second fiber is replaced by the in-line sapphire ball lens interface for coupling from the back side, the peak coupling efficiency drops 1.4 dB (blue curve). For the laterally shifted sapphire and LASF-35 based ball lens interface, the obtained peak coupling efficiency is respectively 2 dB and 2.2 dB lower than the reference. The decrease in coupling efficiency can be explained by taking into account the coupling efficiency of the ball lens interface is not 100% and by the fact that the grating couplers are less efficient for coupling from the back side. The efficiency of grating couplers for interfacing from the back side can further be improved by applying a metal mirror on top of the grating coupler, as we previously demonstrated for grating couplers operating around 1310 nm wavelength [21].

When comparing the coupling efficiencies of the different ball lens interfaces, modest differences were found, which cannot be explained by the difference in theoretical coupling efficiency, being almost the same for the three tested interfaces (cfr. Table 1). Therefore, we assume that the observed differences are caused by positioning inaccuracies of the ball lens with respect to the fiber during the fabrication of the ball lens interfaces and by measurement inaccuracies. Nevertheless, for all tested ball lens configurations, a very limited additional loss was measured when interfacing one of the grating couplers from the bottom side, even without optimizing the grating couplers for back side directionality. Furthermore, if we extract the 2 dB bandwidth of the fiber-to-fiber spectra (which corresponds to the 1 dB bandwidth of a single grating coupler) shown in Figure 4 (i.e. a 2 dB bandwidth of 33 nm for the reference configuration, 32 nm for the in-line sapphire ball lens interface and 31 nm for both shifted ball lens interfaces), there is merely a significant difference.

3.2. Evaluation of the Bragg grating sensor elements

As can be seen in Figure 4, at 22°C, the Bragg wavelength (λ_B = 1536 nm) of the 326 nm pitch sensor does not coincide with the wavelength resulting in peak grating coupling efficiency. Therefore, the coupling angle at which the ball lens interfaces the grating coupler from the back side was increased from 12.5° to 15° to blue-shift the grating coupler spectra and thus to maximize Bragg grating reflectivity. It was verified that this increase in coupling angle did not yield a significantly lower grating coupler peak coupling efficiency. Figure 5 plots the reflection spectra for the reference configuration (black curve) and 3 ball lens configurations. For the reference measurement from the top side using a bare fiber, index matching liquid was used to avoid parasitic reflections, as explained above. Because of the higher refractive index of this liquid (i.e. 1.45) compared to air, the fiber coupling angle was set to 15°/1.45=10.3° to maintain the same coupling conditions. A peak reflectivity of nearly -10 dB was obtained, similarly to what was obtained in transmission (Figure 4). When reading out the Bragg grating sensor with a ball lens, the grating coupler is interfaced 2 times from the back side, so that no direct comparison can be made with the recorded transmission spectra since in that case one of the grating couplers was interfaced from the top side. However, when taking into account the additional loss for a back side interfaced grating coupler, the obtained peak reflectivity values follow the same trend as shown in Figure 4. The envelope 3-dB bandwidth of the reflection spectrum was found to be approximately 5.5 nm, which is much smaller than simulated likely caused by smaller grating corrugation width and smoother corners of the grating sections due to limited fabrication resolution, resulting in a reduce coupling coefficient and hence bandwidth. The difference between peak grating reflectivity and the reflectivity of the first side lobe was found to be 7 dB, which is very close to the simulated value

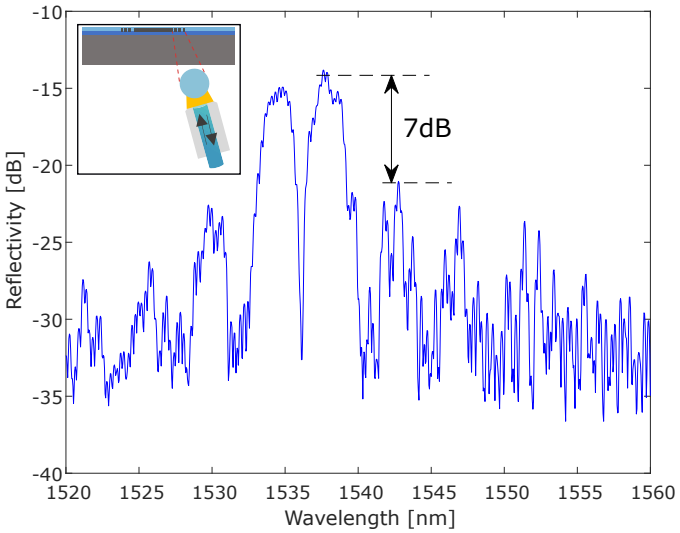

Figure 6: Reflection spectrum of the 326 nm pitch phase shifted Bragg grating temperature sensor recorded at 22°C using the in-line sapphire ball lens interface from the back side (coupling angle 15°).

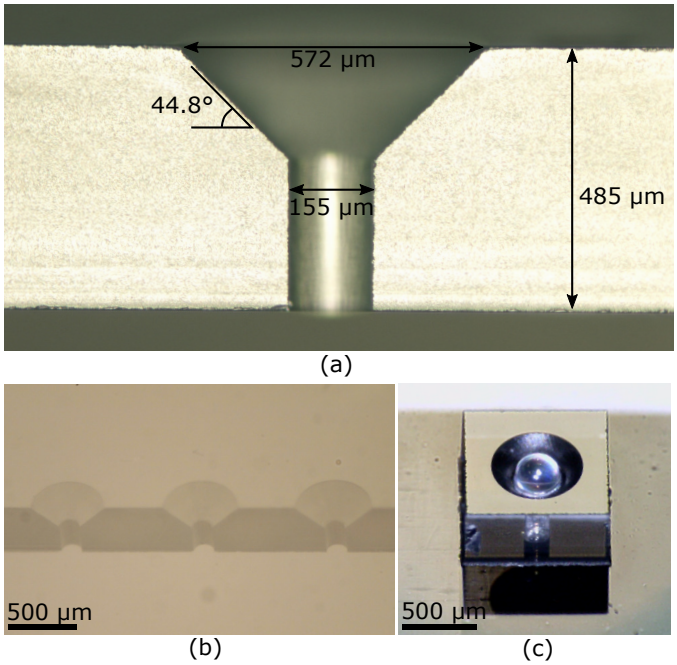

Figure 7: Fabricated ball lens holders in fused silica: (a) Microscopic view on a ball lens holder after cross-sectioning through the centerline; (b) Macroscopic view (after cross-sectioning) on 3 fabricated holder test structures fabricated at different z-coordinates; (c) Macroscopic view on a 300 µm ball lens glued inside a holder.

(i.e. 7.9 dB). This can be seen in Figure 6 showing the reflection spectrum of the sapphire in-line ball lens interface over a wider wavelength range.

3.3. Fabricated holders

Figure 7 shows ball lens holders after the laser inscription and etching process. Figure 7a shows a microscopic view on a cross-sectioned holder revealing that the slope of the conical holder was close to 45°, as intended. By translating the cone in the thickness direction of the glass during the optimization process, the target separation between ball lens and fiber was achieved. This was experimentally verified by writing the 3D design with different vertical offsets (Figure 7b) and selecting the focusing conditions yielding the target design. Figure 7c shows a holder with a glued ball lens after dicing it to the correct dimensions for assembly (970 µm x 970 µm)

3.4. Proof-of-concept sensor demonstration

The process of assembling the sensor probe is illustrated in Figure 8. Figure 8(a) shows the setup used for holding the PIC using a precision gripper to allow aligning it above the fiber ferrule with glued holder and ball lens. Figure 8(b) reveals the individual sub-components, i.e. holder, ball lens, spacer and PIC, after aligning the PIC above the holder but before bringing both components in contact. Finally, Figure 8(c) shows the fully-assembled sensor probe obtained after the aligning and gluing process.

The results of the sensor characterization process are shown in Figure 9 and 10. From Figure 9, it can be seen that the sensor reflection spectra clearly shift to longer wavelengths for increasing temperature. The quality of the signals is slightly worse compared to those presented earlier (see e.g. Figure 5) because the SLED source used inside the interrogator had a relatively low power and was depolarized, i.e. the TE/TM polarization ratio was approximately 50% (to avoid the need of a polarization controller). Nevertheless, the dip (i.e. at the Bragg wavelength) in the reflection spectrum of the phase-shifted Bragg grating can easily be discerned and when plotting the fitted Bragg wavelength as a function of temperature, the sensor transfer function is obtained (see Figure 10). When fitting a linear function through the measured data, a sensitivity of 73 pm/° C was found, which was very close to the simulated sensitivity (i.e. 70 pm/° C) for Bragg gratings in the current technology [22]. Because a Bragg grating sensor with a different pitch (i.e. 324 nm) and from a different position on the wafer was used for this experiment compared to the one used for the above, the Bragg wavelength at room temperature was different. Klimov et al. have demonstrated a sensitivity of 82 pm/° C (5°C–160°C) for an unpackaged PIC with regular (non phase-shifted) silicon waveguide Bragg grating temperature sensors for a Bragg wavelength around 1540nm. This is very close to the value we obtained which can be understood because the same materials and similar waveguide dimensions were used. However, if we compare the achieved temperature sensitivity with that of silica fiber Bragg gratings at a similar Bragg wavelength, i.e. approximately 13 pm/° C [16], we obtained a more than 5 times larger value owing to the much larger thermo-optic coefficient of silicon compared to silica [27].”

4. Conclusions

We demonstrated that using a 300 µm ball lens, it is possible to efficiently interface a silicon photonics grating coupler with a single mode fiber from the back side, through the

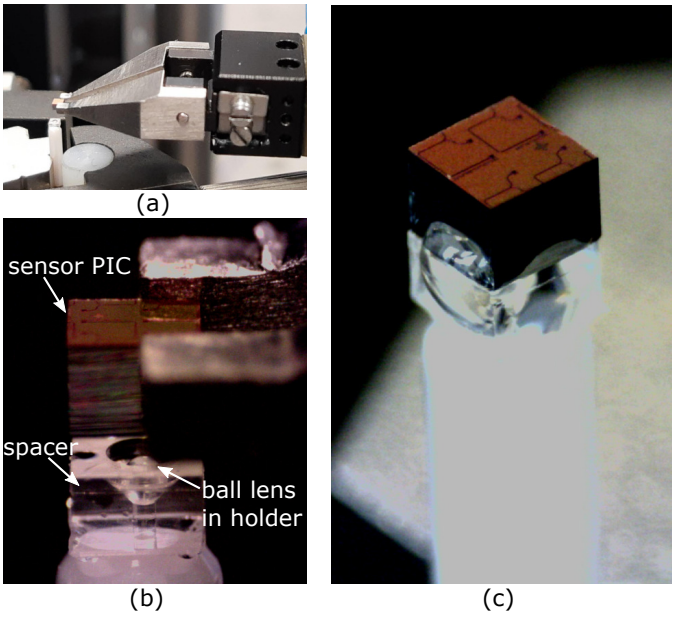

Figure 8: (a) Macroscopic view on the setup used to assemble the sensor PIC on the ferrule; (b) Microscopic view on the sub-components illustrating the 300 µm ball lens glued inside the fused silica holder and the sensor PIC aligned above it; (c) Macroscopic view on the sensor assembly after the gluing process.

thick silicon substrate. The concept was demonstrated employing straight waveguide test structures with TE grating couplers designed for operation around 1550 nm and fabricated using the imec Passives+ MPW service (ISIPP50G). After the standard PIC fabrication process, the only required post-processing steps were polishing of the silicon substrate back side and the application of an anti-reflection coating. Different ball lens configurations were tested employing sapphire and LASF-35 ball lenses, and the measured decrease in peak coupling efficiency when interfacing with a ball lens through the substrate, compared to standard coupling from the top side with a bare fiber ranged between 1.4 and 2.2 dB, without significant decrease in bandwidth. Such a back side interface is very useful for sensing applications since the top side of the PIC remains accessible and since it allows packaging the PIC into a very compact sensor probe. This capability was demonstrated by realizing a phase shifted Bragg grating based temperature sensor probe with an overall diameter less than 1.5 mm. Therefore, precision holders were realized in fused silica glass using a femtosecond laser direct-write technology which allowed to accurately position the ball lens with respect to the interfacing fiber and PIC. After verifying that Bragg grating sensor reflection spectra can be read out using the developed ball lens interface from the back side, a test assembly was made by gluing the holder with ball lens on top of a ferrule and then gluing the sensor PIC on top of the holder. Upon subjecting the sensor probe to increasing temperature, a red shifting of the reflection spectrum was observed as expected. Within the tested range between 15°C and 60°C a, shift in Bragg wavelength of 73 pm/°C was found. Although demonstrated for a temperature sensor probe, we expect that this packaging approach may benefit many other silicon photonics applications.

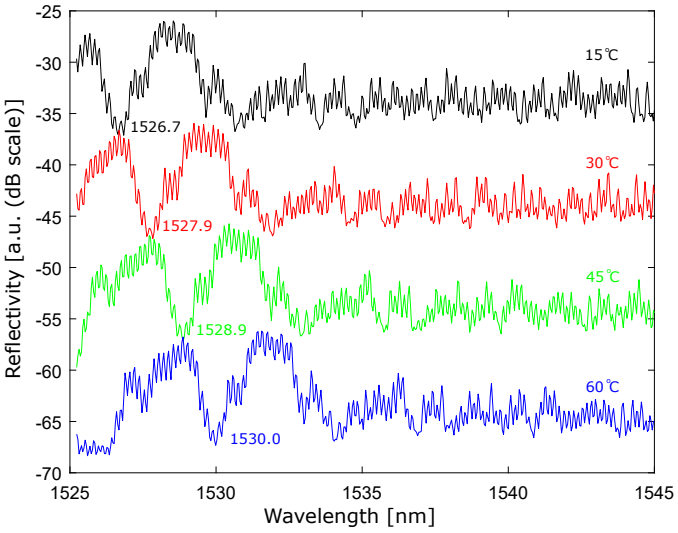

Figure 9: Sensor reflection spectra at 15, 30, 45, 60 ° C for a phase shifted Bragg grating with pitch 324 nm. The different spectra were deliberately offset in the vertical direction for clarity. The extracted Bragg wavelength (in nm) is indicated next to the dip in each spectrum.

Acknowledgment

This work was performed within the SEER project which has received funding from the European Union's Horizon 2020 programme. The authors would also like to thank Stijn Duynslager for the dicing of the PICs, Steven Verstuyft for the application of the silicon nitride anti-reflection coating and Filip Thielemans for help with the realization of the gripper-based assembly setup.

References

[1] Z. Zhou, R. Chen, X. Li, T. Li, Development trends in silicon photonics for data centers, Optical Fiber Technology 44 (2018) 13–23, special Issue on Data Center Communications. doi:https://doi.org/10.1016/j.yofte.2018.03.009.

[2] S. Y. Siew, B. Li, F. Gao, H. Y. Zheng, W. Zhang, P. Guo, S. W. Xie, A. Song, B. Dong, L. W. Luo, C. Li, X. Luo, G.-Q. Lo, Review of silicon photonics technology and platform development, J. Lightwave Technol. 39 (13) (2021) 4374–4389.

[3] Y. Chen, H. Lin, J. Hu, M. Li, Heterogeneously integrated silicon photonics for the mid-infrared and spectroscopic sensing, ACS Nano 8 (7) (2014) 6955–6961, pMID: 24884013. doi:10.1021/nn501765k.

[4] G. Roelkens, A. Abassi, P. Cardile, U. Dave, A. De Groote, Y. De Koninck, S. Dhoore, X. Fu, A. Gassenq, N. Hattasan, Q. Huang, S. Kumari, S. Keyvaninia, B. Kuyken, L. Li, P. Mechet, M. Muneeb, D. Sanchez, H. Shao, T. Spuesens, A. Z. Subramanian, S. Uvin, M. Tassaert, K. Van Gasse, J. Verbist, R. Wang, Z. Wang, J. Zhang, J. Van Campenhout, X. Yin, J. Bauwelinck, G. Morthier, R. Baets, D. Van Thourhout, Iii-v-on-silicon photonic devices for optical communication and sensing, Photonics 2 (3) (2015) 969–1004. doi:10.3390/photonics2030969.

[5] C. V. Poulton, A. Yaacobi, D. B. Cole, M. J. Byrd, M. Raval, D. Vermeulen, M. R. Watts, Coherent solid-state lidar with silicon photonic optical phased arrays, Opt. Lett. 42 (20) (2017) 4091–4094. doi:10.1364/OL.42.004091.

[6] E. Luan, H. Shoman, D. M. Ratner, K. C. Cheung, L. Chrostowski, Silicon photonic biosensors using label-free detection, Sensors 18 (10) (2018). doi:10.3390/s18103519.

[7] N. T. Benéitez, B. Baumgartner, J. Missinne, S. Radosavljevic, D. Wacht, S. Hugger, P. Leszcz, B. Lendl, G. Roelkens, Mid-ir sensing platform for trace analysis in aqueous solutions based on a germanium-on-silicon

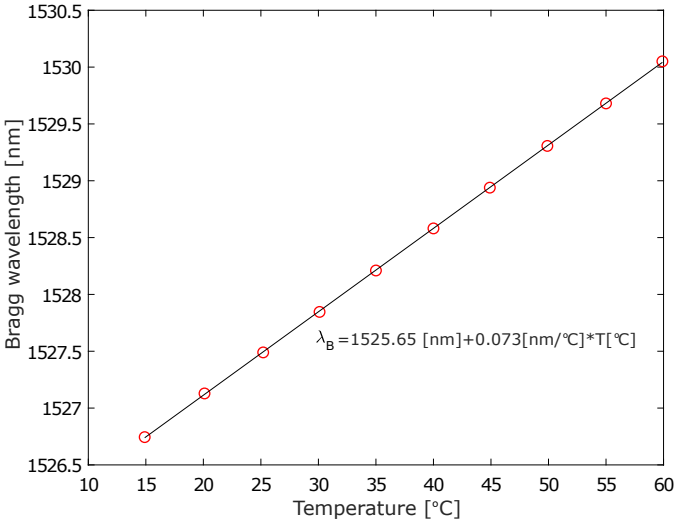

Figure 10: Transfer function of the sensor assembly showing the Bragg wavelength as a function of temperature.

waveguide chip with a mesoporous silica coating for analyte enrichment, Opt. Express 28 (18) (2020) 27013–27027. doi:10.1364/OE.399646.

[8] L. Carroll, J.-S. Lee, C. Scarcella, K. Gradkowski, M. Duperron, H. Lu, Y. Zhao, C. Eason, P. Morrissey, M. Rensing, S. Collins, H. Y. Hwang, P. O'Brien, Photonic packaging: Transforming silicon photonic integrated circuits into photonic devices, Applied Sciences 6 (12) (2016). doi:10.3390/app6120426.

[9] R. Marchetti, C. Lacava, L. Carroll, K. Gradkowski, P. Minzioni, Coupling strategies for silicon photonics integrated chips, Photon. Res. 7 (2) (2019) 201–239. doi:10.1364/PRJ.7.000201.

[10] C. Scarcella, K. Gradkowski, L. Carroll, J.-S. Lee, M. Duperron, D. Fowler, P. O'Brien, Pluggable single-mode fiber-array-to-pic coupling using micro-lenses, IEEE Photonics Technology Letters 29 (22) (2017) 1943–1946. doi:10.1109/LPT.2017.2757082.

[11] M. Duperron, L. Carroll, M. Rensing, S. Collins, Y. Zhao, Y. Li, R. Baets, P. O'Brien, Hybrid integration of laser source on silicon photonic integrated circuit for low-cost interferometry medical device, in: H. Schröder, R. T. Chen (Eds.), Optical Interconnects XVII, Vol. 10109, International Society for Optics and Photonics, SPIE, 2017, pp. 220 – 236. doi:10.1117/12.2250921.

[12] C. Caer, R. Dangel, B. J. Offrein, M. Moehrle, et al., In situ 3d nanoprinting of free-form coupling elements for hybrid photonic integration, Nature Photonics (2018).

[13] J. Missinne, N. T. Benéitez, N. Mangal, J. Zhang, A. Vasiliev, J. V. Campenhout, B. Snyder, G. Roelkens, G. V. Steenberge, Alignment-tolerant interfacing of a photonic integrated circuit using back side etched silicon microlenses, in: G. T. Reed, A. P. Knights (Eds.), Silicon Photonics XIV, Vol. 10923, International Society for Optics and Photonics, SPIE, 2019, pp. 1 – 7. doi:10.1117/12.2506159.

[14] N. Mangal, B. Snyder, J. V. Campenhout, G. V. Steenberge, J. Missinne, Monolithic integration of microlenses on the backside of a silicon photonics chip for expanded beam coupling, Opt. Express 29 (5) (2021) 7601–7615. doi:10.1364/OE.412353.

[15] N. Mangal, J. Missinne, J. Van Campenhout, B. Snyder, G. Van Steenberge, Ball lens embedded through-package via to enable backside coupling between silicon photonics interposer and board-level interconnects, Journal of Lightwave Technology 38 (8) (2020) 2360–2369. doi:10.1109/JLT.2020.2966446.

[16] Y.-J. Rao, In-fibre bragg grating sensors, Measurement Science and Technology 8 (4) (1997) 355–375. doi:10.1088/0957-0233/8/4/002.

[17] J. G. Castelló, V. Toccafondo, P. Pérez-Millán, N. S. Losilla, J. L. Cruz, M. V. Andrés, J. García-Rupérez, Real-time and low-cost sensing technique based on photonic bandgap structures, Opt. Lett. 36 (14) (2011) 2707–2709. doi:10.1364/OL.36.002707.

[18] X. Wang, J. Flueckiger, S. Schmidt, S. Grist, S. T. Fard, J. Kirk, M. Doerfler, K. C. Cheung, D. M. Ratner, L. Chrostowski, A silicon photonic biosensor using phase-shifted bragg gratings in slot waveguide, Journal of Biophotonics 6 (10) (2013) 821–828. doi:10.1002/jbio.201300012.

[19] Ruiz-Tórtola, F. Prats-Quílez, D. González-Lucas, M.-J. Bañuls, Maquieira, G. Wheeler, T. Dalmay, A. Griol, J. Hurtado, H. Bohlmann, R. Götzen, J. García-Rupérez, Experimental study of the evanescent-wave photonic sensors response in presence of molecular beacon conformational changes, Journal of Biophotonics 11 (10) (2018) e201800030. doi:10.1002/jbio.201800030.

[20] N. N. Klimov, S. Mittal, M. Berger, Z. Ahmed, On-chip silicon waveguide bragg grating photonic temperature sensor, Opt. Lett. 40 (17) (2015) 3934–3936. doi:10.1364/OL.40.003934.

[21] N. Mangal, J. Missinne, G. Van Steenberge, J. Van Campenhout, B. Snyder, Performance evaluation of backside emitting o-band grating couplers for 100-µm-thick silicon photonics interposers, IEEE Photonics Journal 11 (3) (2019) 1–11. doi:10.1109/JPHOT.2019.2918522.

[22] C. Zervos, G. Poulopoulos, J. Missinne, M. Szaj, H. Avramopoulos, Miniaturized silicon photonics multi-sensor operating at high temperatures for use in composite materials industrial applications, in: L. E. Busse, Y. Soskind (Eds.), Photonic Instrumentation Engineering IX, Vol. 12008, International Society for Optics and Photonics, SPIE, 2022, pp. 218 – 227. doi:10.1117/12.2606053.

[23] R. Osellame, H. Hoekstra, G. Cerullo, M. Pollnau, Femtosecond laser microstructuring: an enabling tool for optofluidic lab-on-chips, Laser & Photonics Reviews 5 (3) (2011) 442–463. doi:https://doi.org/10.1002/lpor.201000031.

[24] A. Radosavljević, A. Desmet, J. Missinne, K. Saurav, V. Panapakkam, S. Tuccio, C. L. Arce, J. Watté, D. Van Thourhout, G. Van Steenberge, Femtosecond laser-inscribed non-volatile integrated optical switch in fused silica based on microfluidics-controlled total internal reflection, Journal of Lightwave Technology 38 (15) (2020) 3965–3973. doi:10.1109/JLT.2020.2983109.

[25] A. Desmet, A. Radosavljević, J. Missinne, D. Van Thourhout, G. Van Steenberge, Laser written glass interposer for fiber coupling to silicon photonic integrated circuits, IEEE Photonics Journal 13 (1) (2021) 1–12. doi:10.1109/JPHOT.2020.3039900.

[26] M. Haque, P. R. Herman, Chemical-assisted femtosecond laser writing of optical resonator arrays, Laser & Photonics Reviews 9 (6) (2015) 656–665. doi:https://doi.org/10.1002/lpor.201500062.

[27] G. Cocorullo, F. G. Della Corte, I. Rendina, Temperature dependence of the thermo-optic coefficient in crystalline silicon between room temperature and 550 k at the wavelength of 1523 nm, Applied Physics Letters 74 (22) (1999) 3338–3340. doi:10.1063/1.123337.